

PCCP

Accepted Manuscript



This is an *Accepted Manuscript*, which has been through the Royal Society of Chemistry peer review process and has been accepted for publication.

Accepted Manuscripts are published online shortly after acceptance, before technical editing, formatting and proof reading. Using this free service, authors can make their results available to the community, in citable form, before we publish the edited article. We will replace this *Accepted Manuscript* with the edited and formatted *Advance Article* as soon as it is available.

You can find more information about *Accepted Manuscripts* in the [Information for Authors](#).

Please note that technical editing may introduce minor changes to the text and/or graphics, which may alter content. The journal's standard [Terms & Conditions](#) and the [Ethical guidelines](#) still apply. In no event shall the Royal Society of Chemistry be held responsible for any errors or omissions in this *Accepted Manuscript* or any consequences arising from the use of any information it contains.

Benzodi(pyridothiophene): A novel acceptor unit for application in the A₁-A-A₁ type photovoltaic small molecules

Jianhua Chen,^a Manjun Xiao,^{a,b} Linrui Duan,^a Qiong Wang,^a Hua Tan, Ning Su,^a Yu Liu, Renqiang Yang,^{*b} Weiguo Zhu^{*a}

^aCollege of Chemistry, Xiangtan University, Key Lab of Environment-Friendly Chemistry and Application in Ministry of Education, Xiangtan 411105, China

^bQingdao Institute of Bioenergy and Bioprocess Technology, Chinese Academy of Sciences, Qingdao 266101, China

*To whom correspondence should be addressed. Email:

(W. Z.) zhuwg18@126.com

(R. Y.) yangrq@qibebt.ac.cn

Abstract: A series of novel A₁-A-A₁ type small molecules (SMs) of BDPT-2BT, BDPT-2FBT and BDPT-2DPP were designed and synthesized, in which benzodi(pyridothiophene) (BDPT) was used as a novel weak central acceptor (A) unit, as well as benzothiadiazole (BT), fluorinated benzothiadiazole (FBT) and diketopyrrolo pyrrole (DPP) were used as terminal acceptor (A₁) units, respectively. The pentacyclic BDPT aromatic unit can form big conjugated and planar SMs with the A₁ unit, resulting in the enhanced π - π stacking and crystallinity. The effect of the A₁ unit on optical, electrochemical and photovoltaic properties of three SMs was observed. The broader absorption spectrum, lower HOMO energy level, higher photo-response efficiency and better photovoltaic property were exhibited for BDPT-2DPP. The maximum PCE of 3.97% with a V_{oc} of 0.84 V, a J_{sc} of 9.0 mA /cm² and a FF of 52.37% was obtained in BDPT-2DPP/PC₇₁BM-based solar cells, which is 1.8 and 1.5 times values of the BDPT-2BT and BDPT-2FBT-based cells, respectively.

KEYWORDS: Small molecule; Benzodi(pyridothiophene); Diketopyrrolopyrrole; Benzothiadiazole; Photovoltaic property.

1. Introduction

For developing high-efficiency organic photovoltaics (OPVs), in past few years, many building blocks of benzodithiophene, fluorene, carbazole, thienopyrrolo-dione, quinoxaline, diketopyrrolopyrrole, benzothiadiazole and isoindigo are widely used to construct photovoltaic donor materials.¹⁻¹⁰ The modification and improvement of these building blocks, such as fluorination, atom substitution, fused ring-expanding, side chain engineering and so on, have been found to promote the photovoltaic performance for their polymers and small molecules.¹¹⁻¹⁸ Consequently, the power conversion efficiency (PCE) of 10.7%¹⁹ and 10.1%²⁰ for OPVs based on polymers (P-OPVs) and small molecules (SM-OPVs) are achieved, respectively.

Among these building blocks, the lactam derivatives were mostly reported as acceptor units in photovoltaic materials owing to their strong electron-withdrawing ability for forming the intramolecular donor-acceptor electron transfer and the relatively strong interaction between amide groups and fullerenes for efficient charge carrier separation.²¹⁻²³ As a result, the polymers bearing lactam units have showed excellent photovoltaic performance in P-OPVs. For instance, Marks *et al* reported a series of the bithiopheneimide (BTI)-based polymers and presented the maximum PCE of 6.41% for the their OPVs.²¹ Ding group designed a new pentacyclic aromatic lactam (TPTI) as acceptor unit and exhibited a PCE of 7.80% for the TPTI-based polymer in OPVs.²³

As lactam with ambident reactivity is easy to be functionalized by *N*- or *O*- alkylation, Kroon *et al* recently presented an isomer of tetracyclic lactam (NT) building block by *O*-alkylation, which is also regarded as pyridine derivative, and its copolymer showed a PCE of 5% in OPVs.²⁴ Liu *et al* developed a thiophene-fused azacoronene (TAC) unit with bigger conjugate and planar system and its copolymer with mobility up to $0.028 \text{ cm}^2 \text{ V}^{-1} \text{ S}^{-1}$ and a PCE of 4.8% in the inverted device.²⁵ Both fused heterocyclic building blocks of NT and TAC have low electron-withdrawing ability because of the effect of nitrogen atom with sp^2 hybridization in the fused-pyridine rings, which help its copolymers achieve deep highest occupied molecular orbital (HOMO) and its OPVs device obtain high open circuit voltage (V_{oc}).

Furthermore, these copolymers containing NT and TAC units have a remarkable self-organization behavior, which promote their OPVs devices exhibit high fill factor (FF). However, these OPVs devices have not exhibited satisfactory short circuit (J_{sc}) and PCEs values. It is considered to be related to the relatively narrow absorption spectra of these copolymers. Thus, the broader UV-vis absorption spectra with low band-gap and suitable energy levels are needed for the copolymers.

SM-OPVs have many advantages, such as well-defined structures, easier purification, and less batch to batch variation, as compared to P-OPVs. In this work, we focused on multi-heterocyclic building block to construct novel photovoltaic small molecules with broad UV-vis absorption spectra and suitable energy levels. Herein, a novel penta-heterocyclic building block of benzodi(pyridothiophene) (BDPT), i.e. thieno[2',3':4,5]pyrido[2,3-g]thieno[3,2-c]quinoline (Fig. 1) was designed and synthesized via Bischler-Napieralski cyclization. In consideration of the intrinsic relatively low HOMO energy level of the pyridine derivative and requirement of broad absorption spectra for photovoltaic SMs, a series of A_1 -A- A_1 type SMs of BDPT-2BT, BDPT-2FBT and BDPT-2DPP were designed and synthesized, in which BDPT was used as a weak central acceptor (A) unit and benzothiadiazole (BT), fluorinated benzothiadiazole (FBT), diketopyrrolo- pyrrole (DPP) were used as the second strong acceptor (A_1) unit, respectively. In such case, the optical, electrochemical and photovoltaic properties of these SMs can be tuned with the second acceptor unit. As expected, these three SMs showed the enhanced π - π stacking and crystallinity, as well as relatively low HOMO energy levels. BDPT-2DPP exhibited broader absorption spectrum, lower HOMO energy level, higher photo-response efficiency and better photovoltaic property in contrast to BDPT-2BT and BDPT-2FBT. The maximum PCE of 3.97% with a V_{oc} of 0.84 V, a J_{sc} of 9.0 mA/cm² and a FF of 52.37% was obtained in the BDPT-2DPP/PC₇₁BM-based solar cells. Our results demonstrated that benzodi(pyridothiophene) is a promising building block to construct photovoltaic SMs for potential application in solution- processed SM-OPVs.

2. Experimental section

2.1. Materials

All reactions were carried out under nitrogen atmosphere. All reagents and solvents were purchased from Adamas, Sigma and Aldrich corporations. These chemicals were used without further purification unless stated otherwise. Compounds **2-7** and **9-11** were prepared according to the reported procedures.²⁶⁻²⁹

2.2. Measurement and characterization

¹H NMR and ¹³C NMR spectra were recorded on a Bruker Avance-400 spectrometer at 400 MHz and 100 MHz using CDCl₃ as the solvent and tetramethylsilane (TMS) as the internal standard unless specified otherwise, respectively. Mass spectra were measured on a Bruker Daltonics BIFLEX III MALDI-TOF analyzer using MALDI-TOF mode. Crystal-structure were determined on a Nonius KCCD diffractometer with graphite monochromated Mo K radiation. The structures were analyzed by direct methods (SHELXS-97). UV-vis absorption spectra were recorded on a Shimadzu UV-1800 spectrophotometer. Thermogravimetric analysis (TGA) was measured on a Perkin-Elmer Diamond TG/DTA thermal analyzer at scan rate of 10 °C/min under nitrogen atmosphere. The differential scanning calorimetry (DSC) was measured on TA DSCQ-10 instrument at a heating rate of 10 °C/min under nitrogen atmosphere. Cyclic voltammetry (CV) measurement was conducted on a CHI620 voltammetric analyzer under argon atmosphere in an anhydrous acetonitrile solution of tetra(n-butyl) ammonium hexafluorophosphate (0.1 M) at a scan rate of 20 mV/s. A platinum plate, a platinum wire and an Ag/AgCl electrode were used as working electrode, counter electrode, reference electrode, respectively. SMs were coated on the surface of platinum plate and all potentials were corrected against Fc/Fc⁺.

2.3. Device fabrication and characterization

All devices were fabricated on indium tin oxide (ITO)-coated glass substrates, were cleaned by ultrasonic wave with detergent, deionized water, acetone, and isopropyl alcohol, respectively for 20 min. Poly(3,4-ethylenedioxythiophene)/poly(styrenesulfonate) (PEDOT:PSS, Clevios™ P Al 4083) was spin-coated onto ITO glass at 4000 rpm for 30 s and baked at 150 °C for 10 min in air. The solution of SM and PC₇₁BM in chloroform (12 mg/mL) was spin-coated onto PEDOT:PSS layer to form active layer. The thickness of the active layer was approximate 90 nm measured by a

KLA Tencor D-120 profilometer. Ca (10 nm) and Al (100 nm) were deposited successively on active layer by thermal evaporation under a vacuum less than 2×10^{-6} mbar. The active area is 4 mm^2 for each cell. Current density (J)-voltage (V) curves were performed on a Newport 150W solar simulator under AM1.5G illumination with irradiation intensity of 100 mW/cm^2 . The external quantum efficiency (EQE) of the devices was measured on a QE-R3011 solar spectral response measurement system (Enli Technology).

2.4. Synthesis

2.4.1 Synthesis of 2,5-di(thiophen-2-yl)-1,4-bis(2-hexyldecanamido) phenylene (**8**)

To a solution of 2,5-di(thiophen-2-yl)benzene-1,4-diamine (1.2 g, 44.1 mmol) in THF/Et₃N (v/v, 1:1) was added 2-hexyldecanoyl chloride (4.8 g, 175.2 mmol) slowly at 0 °C under stirring. The mixture was then stirred at room temperature for 2 h and poured into water (80 mL). The organic phase was separated and the aqueous solution was extracted with dichloromethane ($2 \times 50 \text{ mL}$). The resulting organic layers were combined and dried over anhydrous MgSO₄. The organic solvent was distilled off and the residue was purified by chromatography on silica gel column using a mixture of dichloromethane (CH₂Cl₂) and petroleum ether (PE) (v/v, 1:1) as eluent to afford compound **8** as a white solid (2.1 g, 63.6%). ¹H NMR (400 MHz, CDCl₃) δ (ppm): 8.45 (s, 2H), 7.48 (s, 2H), 7.45 (d, $J = 3.8 \text{ Hz}$, 4H), 7.19 (s, 2H), 7.15 (d, $J = 3.7 \text{ Hz}$, 2H), 2.05 (s, 2H), 1.42 (s, 8H), 1.24 (s, 40H), 0.86 (s, 12H). ¹³C NMR (100 MHz, CDCl₃) δ (ppm): 174.38, 138.44, 131.28, 127.75, 127.50, 127.00, 125.00, 123.62, 49.30, 33.18, 31.85, 31.70, 29.70, 29.46, 29.36, 29.28, 27.66, 27.62, 22.66, 22.62, 14.10, 14.06. Elemental analysis for C₄₆H₇₂N₂O₂S₂: calcd. C, 73.74; H, 9.69; N, 3.74; found C, 73.53; H, 9.38; N, 3.94.

2.4.2 Synthesis of 4,10-di(pentadecan-7-yl)thieno[2',3':4,5] pyrido[2,3-g]thieno[3,2-c]quinoline (**BDPT**)

Compound **8** (1.5 g, 2.0 mmol) and P₂O₅ (1 g, 8.9 mmol) in freshly distilled POCl₃ (40 mL) was stirred at reflux for 6 h under N₂. The solvent was distilled under a high vacuum, the residue was cooled to room temperature and transferred slowly to ice water (100 mL). The mixture was neutralized to pH = 10 with NaOH solution (2M)

and then extracted with CHCl_3 (3×30 mL). The combined organic layers were dried over anhydrous MgSO_4 and distilled to remove off the solvent. The residue was purified by chromatography on silica gel column using CH_2Cl_2 -PE (v/v , 1:5) as eluent and recrystallization from ethanol to afford **BDPT** as a light yellow solid (1.1 g, 77.0%). ^1H NMR (400 MHz, CDCl_3) δ (ppm): 8.92 (s, 2H), 7.72 (d, $J = 5.2$ Hz, 2H), 7.60 (d, $J = 5.2$ Hz, 2H), 3.42 (dd, $J = 12.0, 6.7$ Hz, 2H), 2.18-2.05 (m, 6H), 1.92-1.70(m, 10H), 1.23 (d, $J = 32.3$ Hz, 22 H), 0.82 (t, $J = 6.3$ Hz, 12H). ^{13}C NMR (100 MHz, CDCl_3) δ (ppm): 163.28, 144.96, 141.64, 133.30, 125.74, 124.02, 123.98, 122.90, 46.32, 35.14, 35.12, 31.82, 31.70, 29.84, 29.52, 29.42, 29.20, 27.96, 27.94, 22.58, 22.56, 13.98, 13.96. MS (MALDI-TOF) for $\text{C}_{46}\text{H}_{68}\text{N}_2\text{S}_2$: 714.525 $[\text{M}+\text{H}]^+$. Elemental analysis for $\text{C}_{46}\text{H}_{68}\text{N}_2\text{S}_2$: calcd. C, 77.47; H, 9.61; N, 3.93; found C, 74.08; H, 9.97; N, 3.77.

2.4.3 Synthesis of 4,10-di(pentadecan-7-yl)-2,8-bis(trimethylstannyl)thieno[2',3':4,5]pyrido[2,3-g]thieno[3,2-c]quinoline (**M1**)

To a solution of compound **BDPT** (1.4 g, 2.0 mmol) in THF(100 mL) at -78 °C was added dropwise 2 mL of n-butyllithium (4.4 mmol, 2.5 M in n-hexane) under stirring and a nitrogen atmosphere. After being stirred at -78 °C for 1 h, a great deal of yellow solid precipitate appeared. Then, 4.4 mL of trimethyltin chloride (4.4 mmol, 1M in n-hexane) was added in one portion, and the mixture turned to clear rapidly. Allowed it warm up to ambient temperature and the reactant was stirred for 2 h. Poured it into 200 mL of cool water and the mixture was extracted by ether (3×50 mL). The organic layer was washed by water two times and then dried over anhydrous MgSO_4 . After removed off solvent under vacuum, the residue was recrystallized by ethanol, Compound **M1** was obtained as pale yellow crystal (1.5 g, yield 72.5%) . ^1H NMR (400 MHz, CDCl_3) δ (ppm): 8.93 (s, 2H), 7.80-7.70 (m, 2H), 3.48 (s, 2H), 2.09 (t, $J = 21.8$ Hz, 6H), 1.86 (s, 6H), 1.60-1.16 (m, 36H), 0.89-0.73 (m, 12H), 0.48 (d, $J = 28.2$ Hz, 18H). ^{13}C NMR (100 MHz, CDCl_3) δ (ppm): 163.92, 149.86, 141.26, 139.88, 134.66, 131.64, 123.78, 123.06, 46.08 (, 35.08, 35.04, 31.88, 31.76, 29.92, 29.58, 29.48, 29.28, 27.94, 27.92, 22.64, 22.62, 14.08, 14.06, -8.04. MS (MALDI-TOF) for $\text{C}_{52}\text{H}_{84}\text{N}_2\text{S}_2\text{Sn}_2$: 1039.465 $[\text{M}+\text{H}]^+$. Elemental analysis for $\text{C}_{52}\text{H}_{84}\text{N}_2\text{S}_2\text{Sn}_2$: calcd. C, 60.12; H, 8.15; N, 2.70; found C, 60.12; H, 7.94; N, 2.82.

2.4.4 Synthesis of **BDPT-2BT**

To a solution of compound **9** (164.4 mg, 0.3 mmol) and **M1** (155.7 mg, 0.15 mmol) in toluene (10 mL) were added tris(dibenzylideneacetone) dipalladium ($\text{Pd}_2(\text{dba})_3$, 6 mg) and tri-*o*-tolylphosphine (12 mg) under a nitrogen atmosphere. The mixture was stirred at 110 °C for 6 h. Allowed the reaction solution cool down to ambient temperature, the mixture was poured into 100 mL water and extracted with CH_2Cl_2 (100 mL). The resulting organic phase was collected and dried over anhydrous MgSO_4 . After the solvent was distilled by rotary evaporation and the residue was purified by chromatography on a silica gel column using CH_2Cl_2 -PE (*v/v*, 3:1) as eluent to give red solid (202.2 mg, yield 82.1%). ^1H NMR (400 MHz, CDCl_3) δ (ppm): 8.85 (s, 2H), 8.04 (d, $J = 12.0$ Hz, 4H), 7.88 (s, 4H), 7.74 (s, 2H), 7.08 (s, 2H), 3.52 (s, 2H), 3.03 (s, 4H), 2.72 (s, 4H), 2.22 (s, 4H), 2.04-0.99 (m, 76H), 0.99-0.86 (m, 24H). MS (MALDI-TOF) for $\text{C}_{98}\text{H}_{128}\text{N}_6\text{S}_8$: 1647.125[M+H]⁺. Elemental analysis for $\text{C}_{98}\text{H}_{128}\text{N}_6\text{S}_8$: calcd. C, 71.48; H, 7.84; N, 5.10; found C, 71.72; H, 7.71; N, 5.12.

2.4.5 Synthesis of **BDPT-2FBT**

To a solution of compound **10** (175.2 mg, 0.3 mmol) and **M1** (155.7 mg, 0.15 mmol) in toluene (10 mL) were added $\text{Pd}_2(\text{dba})_3$ (6 mg) and tri-*o*-tolylphosphine (12 mg) under a nitrogen atmosphere. The synthetic procedures were the same as the synthesis of **BDPT-2BT**. The product was purified by chromatography on a silica gel column using CH_2Cl_2 -PE (*v/v*, 2.5:1) as eluent to give red solid (201.5 mg, yield 78.2%). ^1H NMR (400 MHz, CDCl_3) δ (ppm): 8.52 (s, 2H), 8.08 (s, 2H), 8.01 (s, 2H), 7.43 (s, 2H), 7.05 (s, 2H), 3.48-3.41 (m, 2H), 2.96 (t, $J = 7.2$ Hz, 4H), 2.60 (t, $J = 6.8$ Hz, 4H), 2.24 (d, $J = 6.0$ Hz, 4H), 1.98 (s, 4H), 1.86 (dd, $J = 14.5, 7.4$ Hz, 4H), 1.62 (s, 10H), 1.54-1.20 (m, 54H), 1.00 (t, $J = 6.5$ Hz, 6H), 0.92-0.83 (m, 18H). MS (MALDI-TOF) for $\text{C}_{98}\text{H}_{128}\text{F}_4\text{N}_6\text{S}_8$: 1719.297[M+H]⁺. Elemental analysis for $\text{C}_{98}\text{H}_{128}\text{F}_4\text{N}_6\text{S}_8$: calcd. C, 68.49; H, 7.27; N, 4.89; found C, 68.60; H, 7.31; N, 4.82.

2.4.6 Synthesis of **BDPT-2DPP**

To a solution of compound **11** (127.2 mg, 0.2 mmol) and **M1** (103.8 mg, 0.1 mmol) in toluene (10 mL) were added $\text{Pd}_2(\text{dba})_3$ (5 mg) and tri-*o*-tolylphosphine (10 mg) under a nitrogen atmosphere. The synthetic procedures were the same as the synthesis

of **BDPT-2BT**. The product of **BDPT-2DPP** was purified by chromatography on a silica gel column using CH₂Cl₂-PE (v/v, 2:1) as eluent to give blue solid (126.1 mg, yield 72.2%). ¹H NMR (400 MHz, CDCl₃) δ(ppm): 8.99 (d, *J* = 3.9 Hz, 2H), 8.92 (d, *J* = 3.2 Hz, 2H), 8.59 (s, 2H), 7.72 (s, 2H), 7.58 (d, *J* = 4.1 Hz, 2H), 7.41 (s, 2H), 7.24 (d, *J* = 4.1 Hz, 2H), 4.06 (d, *J* = 5.6 Hz, 8H), 3.43 (d, *J* = 5.5 Hz, 2H), 2.17 (d, *J* = 7.7 Hz, 4H), 1.93 (s, 10H), 1.50-1.10 (m, 70H), 0.99-0.68 (m, 36H). MS (MALDI-TOF) for C₁₀₆H₁₄₄N₆O₄S₆: 1758.075 [M+H]⁺. Elemental analysis for C₁₀₆H₁₄₄N₆O₄S₆: calcd. C, 72.93; H, 8.25; N, 4.78; found C, 72.53; H, 7.86; N, 4.49.

3. Results and discussion

3.1 synthesis

The synthetic route of three SMs was shown in scheme 1. Compound 7 reacted with 2-hexyldecanoyl chloride in a mixing solvent of THF and Et₃N at 0 °C to give compound 8 with a moderate yield of 63%. The key intermediate of BDPT was obtained by a reaction between compound 8 and condensation reagents of P₂O₅ and POCl₃ with a yield of 77%, which is called as Bischler-Napieralski cyclization. The structure of BDPT was characterized by single crystal X-ray diffraction. M1 were synthesized from BDPT in the presence of n-BuLi and Me₃SnCl at -78°C. The target SMs of BDPT-2BT, BDPT-2FBT and BDPT-2DPP were synthesized via Still coupling reaction of M1 and compound 9, 10, 11 with a yield over 70%, respectively. The structures of these target SMs were characterized by ¹H NMR, MS, elemental analysis.

3.2 Crystal structure of BDPT.

Single crystal of BDPT was grown by slow diffusion of MeOH into the concentrated BDPT solution in CHCl₃. Crystal structure of BDPT was determined and the crystallographic data are provided in Supporting Information. The CIF file can be free obtained from The Cambridge Crystallographic Data Centre www.ccdc.cam.ac.uk/data_request/cif with the CCDC number of 1412263 and listed in Supporting Information. As observed, BDPT belongs to *P*-1 space group of triclinic system with $\alpha = 84.894^\circ$, $\beta = 88.701^\circ$, $\gamma = 72.509^\circ$. As shown in Fig. 1, BDPT exhibits good

planarity and π - π stacking with a distance of 3.468 Å, which will promote the charge transfer when used as a building block in photovoltaic materials.

3.3 Thermal properties.

The thermal behavior of three BDPT-based SMs was evaluated by thermogravimetric analysis (TGA) and differential scanning calorimetry (DSC) measurement. Fig. 2a and Fig. 2b show the recorded TGA and DSC curves, respectively. The detail data were outlined in Table S1. As depicted in Fig. 2a, the decomposition temperature (T_d) of 447 °C, 451 °C and 423 °C are observed for BDPT-2BT, BDPT-2FBT and BDPT-2DPP at 5% weight loss, respectively. These high T_d values may originate from the relative high crystallinity and intermolecular interaction. On the other hand, an endothermic peak under the heating process and an exothermic peak under the cooling process are observed for the three BDPT-based SMs in Fig. 2b, which correspond to the melting temperature (T_m) and crystallization temperature (T_c), respectively. By comparison, it is found that both BDPT-2FBT and BDPT-2DPP exhibited significantly increased T_m and T_c than BDPT-2BT. Therefore, introducing F atom and turning the second acceptor from BT to DPP unit have a significantly positive influence on thermal stability and crystallinity.

3.4. Optical properties

The UV-vis absorption spectra of BDPT-based SMs in chloroform solution (10^{-5} M) and in their thin films are shown in Fig. 3. The detail data are outlined in Table 1. Two distinct absorption bands at a high-lying region from 300-400 nm and a low-lying region from 400-700 nm are observed for these BDPT-based SMs in solution and solid state. An absorption maxima is displayed at 492 nm with a molar extinction coefficient (ϵ) of $7.2 \times 10^4 \text{ M}^{-1} \text{ cm}^{-1}$ for BDPT-2BT solution and at 482 nm with a ϵ value of $1.02 \times 10^5 \text{ M}^{-1} \text{ cm}^{-1}$ for BDPT-2FBT solution. Compared to BDPT-2BT, BDPT-2FBT show a clear blue-shifted absorption profile in solution and solid state due to the electron-withdrawing effect of the fluorine atom.³⁰ While the BT unit is replaced by the DPP unit in the BDPT-based SMs, BDPT-2DPP shows broader absorption profile than BDPT-2BT and BDPT-2FBT due to the stronger electron-deficient ability of DPP than BT and FBT, which result in the stronger intramolecular

charge transfer (ICT) effect. The absorption maxima is appeared at 600 nm with an increasing ϵ value of $8.4 \times 10^5 \text{ M}^{-1} \text{ cm}^{-1}$ for BDPT-2DPP in solution. In contrast to the absorption profiles in solution, those ones in the neat films for these three BDPT-based SMs come up a remarkably red-shifted by about 60 nm due to the strong intermolecular interactions. Furthermore, a new shoulder peak is occurred in the long-wavelength for the three BDPT-based SMs, which results from vibronic coupling due to rigid planar conjugated structure enforced by the molecular packing. The optical band gaps (E_g^{opt}) estimated from the absorption edges (652 nm, 630 nm, 710 nm) of the thin films are 1.90, 1.97 and 1.75 eV for BDPT-2BT, BDPT-2FBT and BDPT-2DPP, respectively. As observed, the E_g^{opt} values of this kind of SMs were governed by the electron-deficient ability of the second acceptor units.

3.5. Electrochemical properties

The electrochemical properties of the BDPT-based SMs were evaluated by cyclic voltammetry (CV) method. The resulting CV curves are shown in Fig.4 and their detail data are summarized in Table 1. The reversible oxidation waves are observed with the onset oxidation potentials (E_{ox}) of 1.01 V, 1.18 V and 1.07 V vs Ag/AgCl electrode for BDPT-2BT, BDPT-2FBT and BDPT-2DPP, respectively. However, the reductive waves were not appeared. As the potential of Fc/Fc⁺ vs Ag/AgCl electrode was measured to be 0.43 V in this work, the HOMO energy levels (E_{HOMO}) of the BDPT-based SMs can be calculated by the following equation: $E_{\text{HOMO}} = -(E_{\text{ox}} + 4.37)$ eV.³¹ As a result, the E_{HOMO} values of BDPT-2BT, BDPT-2FBT and BDPT-2DPP are -5.38 eV, -5.55 eV and -5.44 eV, respectively. Therefore, turning the second acceptor unit from BT to FBT and DPP can make their SMs exhibit lower HOMO energy level.

3.6. Theoretical calculation

Optimal conformations of the three BDPT-based SMs were obtained by molecular modelling on Gaussian 09 at the B3LYP/6-31G* level of theory in the gas phase. To minimize the calculation process, the long alkyl chains were substituted with methyl groups during the calculation. The optimized molecular geometries are depicted in Fig. 5. The backbone of three SMs displays good planarity with a small torsion angle of

2.01°, 2.65° and 0.91° between the strong acceptor unit (BT, FBT and DPP) and the center BDPT unit for BDPT-2BT, BDPT-2FBT and BDPT-2DPP, respectively. The resulting planar structure can facilitate π - π stacking and charge transfer. The calculated frontier orbital distribution of the HOMO and the LUMO for SMs are presented in Figure S1. For BDPT-2BT and BDPT-2FBT, the HOMOs are well delocalized along the backbones of SMs, while the LUMOs are localized on the second of acceptors of BT and FBT units. However, both HOMO and LUMO are delocalized along the backbones for BDPT-2DPP. As the localization can hinder interchain electron transport, since hopping requires good alignment of the localized LUMO levels,³²⁻³⁵ the stronger delocalization of both the HOMO and LUMO for BDPT-2DPP, is expected to enhance intermolecular interactions and improve charge transportation than BDPT-2BT and BDPT-2FBT.

3.6. Photovoltaic properties

Bulk heterojunction (BHJ) solar cells based on SMs and PC₇₁BM were fabricated. The SMs/PC₇₁BM ratios from 1:2, 1:1 to 2:1 and solvent additive of 1,8-diiodooctane (DIO) from 0% to 1% were selected to optimize device performance in active layer. Table S2 summarized the corresponding photovoltaic parameters of the SMs/PC₇₁BM-based devices under illumination of AM 1.5, 100 mW cm⁻². The corresponding J - V curves and the dark currents in the J - V curves for BDPT-based solar cells were displayed in Fig. S2-4. It is found that the optimized SMs/PC₇₁BM ratio is 1:1. Introducing 1% DIO additive is available to improve photovoltaic properties of the BDPT-2DPP-based devices, but decrease photovoltaic properties of the BDPT-2BT- and BDPT-2FBT-based devices. Fig.6 shows the typical J - V curves of the SMs:PC₇₁BM-based devices in this optimized SMs/PC₇₁BM ratio and solvent additive conditions. We find that the BDPT-2DPP- based devices exhibited better photovoltaic properties than the BDPT-2BT- and BDPT-2FBT-based devices. The maximum PCE of 3.09% with a V_{oc} of 0.84 V, a J_{sc} of 8.0 mA/cm² and a FF of 52.37% was obtained in the BDPT-2DPP-based devices at the SMs/PC₇₁BM ratio of 1:1. It indicates that turning the second acceptor unit from BT to FBT and DPP can improve the photovoltaic property for these A₁-A-A₁ type SMs.

For further tuning photovoltaic properties of this type of SMs with A₁-A-A₁ framework, the BDPT-2DPP-based device with the BDPT-2DPP/PC₇₁BM ratio of 1.5:1 and 1% DIO additive was specially made. The increasing PCE of 3.97% with a V_{oc} of 0.84 V, a J_{sc} of 9.0 mA/cm² and a FF of 52.37% was obtained in the cell. The corresponding $J-V$ curve is also shown in Fig. 6. The improved photovoltaic data of three SMs-based devices at optimized process conditions are finally summarized in Table 2. It shows that the PCE value of the BDPT-2DPP-based device is 1.5 times value of the BDPT-2FBT-based device.

The measurement of X-ray diffraction, photo response efficiency and hole mobility further supports why BDPT-2DPP-based device presented best photovoltaic properties among these A₁-A-A₁ type SMs-based devices. Fig. 7 shows the X-ray diffraction patterns of the SMs:PC₇₁BM blend films with/without DIO additive. A clear and intense diffraction peak is respectively observed in the BDPT-2FBT and BDPT-2DPP blend films, while the BDPT-2BT blend film displays a weak diffraction peak around $2\theta = 5^\circ$, which is ascribed to the diffraction between the molecular conjugated backbones separated by the branched alkyl chains. It implies that BDPT-2FBT and BDPT-2DPP have better crystallinity and self-organization than BDPT-2BT, which is well consistent with the DSC results. When 1% DIO additive is added into the SMs:PC₇₁BM blend films, the diffraction peaks are disappeared for BDPT-2BT and weakened for BDPT-2FBT and enhanced for BDPT-2DPP in their blend films. It indicates that the organized nano-structure was disarranged in the BDPT-2BT and BDPT-2FBT blend films with 1% DIO additive, which results in the reduced PCE value. In contrast, more ordered nano-structure was formed in the BDPT-2DPP blend film with 1% DIO additive. As a result, adding 1% DIO additive can significantly increase PCE and J_{sc} values of the BDPT-2DPP-based device.

The influence of 1% DIO additive on the film morphologies were further investigated in these blend films at the optimized ratio between the SM and PC₇₁BM by transmission electron microscopy (TEM) measurement. As shown in Fig. 8, BDPT-2BT and BDPT-2FBT-based blend films display homogeneous morphologies, but the BDPT-2DPP-based blend film reveals serious phase separation morphology without

DIO additive. In contrast, when 1% DIO is added, inhomogeneous morphology and severe phase-segregation phenomenon are formed in the above blend films with BDPT-2BT and BDPT-2FBT. However, homogeneous morphology with cloud-like structure appears in the BDPT-2DPP-based blend film under 1% DIO additive. Therefore, adding 1% DIO additive can improve the morphology of the BDPT-2DPP-based blend film, but destroy the homogeneousness of the BDPT-2BT and BDPT-2FBT-based blend films. In general, the inhomogeneous morphology for photo-active layer may cause more geminate recombination and bimolecular recombination, which can decrease the device J_{sc} value. Proper phase separation and interpenetrating network are benefit for the exciton separation and charge transport, which can promote the device J_{sc} value. This is why the BDPT-2BT and BDPT-2FBT-based devices exhibited the decreased photovoltaic performances, but the BDPT-2DPP-based devices presented the improved ones by adding DIO additive.

Fig. 9 and Fig. 10 show the EQE curves of three SMs:PC₇₁BM blend films and the $J-V$ characteristics of the hole-only devices with the SMs:PC₇₁BM-based active layer, respectively. Although a similar photo response region from 300 to 650 nm is exhibited for BDPT-2BT, BDPT-2FBT blend films, the photo response efficiencies are remarkably different. The highest EQE values of 37.5% and 45.9% are exhibited in the BDPT-2BT and BDPT-2FBT blend films, respectively. In comparison, BDPT-2DPP showed a broader photo response region from 300 to 710 nm with highest EQE values of 50.6%. These calculated J_{sc} values by integration of the EQE data have only 2%-5% mismatch compared with the J_{sc} values from the $J-V$ curve. It indicates that the photoelectron conversion process is more efficient for BDPT-2DPP-based device, which is responsible for the increase of J_{sc} .

Fig. 10 displays $J-V$ characteristics of the hole-only devices in dark, in which the device structure is ITO/PEDOT/SMs:PC₇₁BM/MoO₃/Al. The hole mobility was measured using a space charge limited current (SCLC) method. The hole mobility of 2.94×10^{-6} , 1.66×10^{-5} and 1.05×10^{-4} cm²v⁻¹s⁻¹ are presented for BDPT-2BT, BDPT-2FBT and BDPT-2DPP, respectively. It is obvious that the hole mobility of BDPT-

2DPP increases one order of magnitude compared with that of BDPT-2FBT, which is consistent to the improvement of J_{sc} and FF for the BDPT-2DPP-based device.

Conclusions

In conclusion, three novel A_1 -A- A_1 type SMs of BDPT-2BT, BDPT-2FBT and BDPT-2DPP were obtained, which contain a weak and a strong electron-withdrawing acceptor units. All of them exhibited good planarity and crystallinity, as well as low HOMO energy level. Therein, BDPT-2DPP showed broader absorption spectrum and higher photo response efficiency than BDPT-2BT and BDPT-2FBT. The maximum PCE of 3.97% with a V_{oc} of 0.84 V, a J_{sc} of 9.0 mA /cm² and a FF of 52.37% was obtained in the BDPT-2DPP/PC₇₁BM-based device. This PCE value is 1.8 and 1.5 times of the BDPT-2BT- and BDPT-2FBT-based devices, respectively. Our work demonstrates that BDPT is a promising weak electron-withdrawing building block for design of the photovoltaic SMs. Tuning the second acceptor unit from BT to DPP can significantly improve the photovoltaic property for the A_1 -A- A_1 type SMs.

Acknowledgements

Thanks to the financial supports from the Major Cultivation and General Programs of the National Natural Science Foundation of China (91233112, 21172187, 51403178), the Scientific Research Fund of Hunan Provincial Education Department (10A119), the Innovation Group and Xiangtan Joint Project in Hunan Natural Science Foundation (12JJ7002 and 12JJ8001), the Natural Science Foundation of Hunan (14JJ4019), Open Project for the National Key Laboratory of Luminescent Materials and Devices (2014-skllmd-10), Research Foundation of Hunan Education Bureau (13A102, 14C1099), the Hunan Postgraduate Science Foundation for Innovation (CX2014B257, CX2013B268) and the Natural Science Foundation of Xiangtan University (13QDZ23).

Supporting Information

The detailed data of the optimal BHJ solar cells and their corresponding J - V curves, the NMR spectra, MALDI-MS data and crystal data are shown in Supporting Information, which is available from www.rsc.org or from the author.

References

1. M. Li, W. Ni, X. Wan, Q. Zhang, B. Kan and Y. Chen, *J. Mater. Chem. A*, 2015, **3**, 4765-4776.
2. S. Qu and H. Tian, *Chem Commun*, 2012, **48**, 3039-3051.
3. L. Ye, S. Zhang, L. Huo, M. Zhang and J. Hou, *Accounts Chem. Res.*, 2014, **47**, 1595-1603.
4. J. Chen and Y. Cao, *Accounts Chemical Res.*, 2009, **42**, 1709-1718.
5. Y. J. Cheng, S. H. Yang and C. S. Hsu, *Chem. Rev.*, 2009, **109**, 5868 - 5923
6. R. S. Kularatne, H. D. Magurudeniya, P. Sista, M. C. Biewer and M. C. Stefan, *J. Polymer Sci. Part A: Polymer Chem.*, 2013, **51**, 743-768.
7. Y. Lin, H. Fan, Y. Li and X. Zhan, *Adv. Mater.*, 2012, **24**, 3087-3106, 3081.
8. E. Wang, W. Mammo and M. R. Andersson, *Adv. Mater.*, 2014, **26**, 1801-1826.
9. D. H. Wang, A. Pron, M. Leclerc and A. J. Heeger, *Adv. Funct. Mater.*, 2013, **23**, 1297-1304.
10. H. Choi, S. J. Ko, T. Kim, P. O. Morin, B. Walker, B. H. Lee, M. Leclerc, J. Y. Kim and A. J. Heeger, *Adv. Mater.*, 2015, DOI: 10.1002/adma.201501132.
11. Y.-J. Cheng, J.-S. Wu, P.-I. Shih, C.-Y. Chang, P.-C. Jwo, W.-S. Kao and C.-S. Hsu, *Chem. Mater.*, 2011, **23**, 2361-2369.
12. H. Zhou, L. Yang, A. C. Stuart, S. C. Price, S. Liu and W. You, *Angew. Chem. Int. Ed. Engl.*, 2011, **50**, 2995-2998.
13. T. L. Nguyen, H. Choi, S.-J. Ko, M. A. Uddin, B. Walker, S. Yum, J.-E. Jeong, M. H. Yun, T. J. Shin, S. Hwang, J. Y. Kim and H. Y. Woo, *Energy Environ. Sci.*, 2014, **7**, 3040-3051.
14. M. Zhang, Y. Gu, X. Guo, F. Liu, S. Zhang, L. Huo, T. P. Russell and J. Hou, *Adv. Mater.*, 2013, **25**, 4944-4949.
15. D. Gedefaw, M. Tassarolo, W. Zhuang, R. Kroon, E. Wang, M. Bolognesi, M. Seri, M. Muccini and M. R. Andersson, *Polym. Chem.*, 2014, **5**, 2083-2093.
16. L. Huo, T. Liu, X. Sun, Y. Cai, A. J. Heeger and Y. Sun, *Adv. Mater.*, 2015, DOI: 10.1002/adma.201500647.
17. J.-S. Wu, Y.-J. Cheng, T.-Y. Lin, C.-Y. Chang, P.-I. Shih and C.-S. Hsu, *Adv. Funct. Mater.*, 2012, **22**, 1711-1722.
18. N. Chakravarthi, K. Kranthiraja, M. Song, K. Gunasekar, P. Jeong, S.-J. Moon, W. Suk Shin, I.-N. Kang, J. W. Lee and S.-H. Jin, *Sol. Energy Mater. Sol. C*, 2014, **122**, 136-145.

19. Y. Liu, J. Zhao, Z. Li, C. Mu, W. Ma, H. Hu, K. Jiang, H. Lin, H. Ade and H. Yan, *Nat. commun.*, 2014, **5**, 5293.
20. B. Kan, M. Li, Q. Zhang, F. Liu, X. Wan, Y. Wang, W. Ni, G. Long, X. Yang, H. Feng, Y. Zuo, M. Zhang, F. Huang, Y. Cao, T. P. Russell and Y. Chen, *J. Am. Chem. Soc.*, 2015, **137**, 3886-3893.
21. X. Guo, N. Zhou, S. J. Lou, J. W. Hennek, R. Ponce Ortiz, M. R. Butler, P. L. Boudreaault, J. Strzalka, P. O. Morin, M. Leclerc, J. T. Lopez Navarrete, M. A. Ratner, L. X. Chen, R. P. Chang, A. Facchetti and T. J. Marks, *J. Am. Chem. Soc.*, 2012, **134**, 18427-18439.
22. M. Liu, Y. Liang, P. Chen, D. Chen, K. Liu, Y. Li, S. Liu, X. Gong, F. Huang, S.-J. Su and Y. Cao, *J. Mater. Chem. A*, 2014, **2**, 321-325.
23. J. Cao, Q. Liao, X. Du, J. Chen, Z. Xiao, Q. Zuo and L. Ding, *Energy Environ. Sci.*, 2013, **6**, 3224-3228.
24. R. Kroon, A. D. Z. Mendaza, S. Himmelberger, J. Bergqvist, O. Bañcke, G. C. Faria, F. Gao, A. Obaid, W. Zhuang, D. Gedefaw, E. Olsson, O. Inganäs, A. Salleo, C. Müller and M. R. Andersson, *J. Am. Chem. Soc.*, 2014, **136**, 11578-11581.
25. B. He, A. B. Pun, L. M. Klivansky, A. M. McGough, Y. Ye, J. Zhu, J. Guo, S. J. Teat and Y. Liu, *Chem. Mater.*, 2014, **26**, 3920-3927.
26. D. Wilson, B. Djukic and M. T. Lemaire, *Transition Metal. Chem.*, 2013, **39**, 17-24.
27. J. Chen, M. Xiao, F. Meng, L. Duan, H. Tan, Y. Wang, Y. Liu, R. Yang and W. Zhu, *Syn. Met.*, 2015, **199**, 400-407.
28. Y. Zhang, X. Bao, M. Xiao, H. Tan, Q. Tao, Y. Wang, Y. Liu, R. Yang and W. Zhu, *J. Mater. Chem. A*, 2015, **3**, 886-893.
29. P. Zhou, D. Dang, M. Xiao, Q. Wang, J. Zhong, H. Tan, Y. Pei, R. Yang and W. Zhu, *J. Mater. Chem. A*, 2015, **3**, 10883-10889.
30. Q. Yin, J. Miao, Z. Wu, Z. Chang, J. Wang, H. Wu and Y. Cao, *J. Mater. Chem. A*, 2015, **3**, 11575-11586.
31. C. Cui, W.-Y. Wong and Y. Li, *Energy Environ. Sci.*, 2014, **7**, 2276-2284.
32. C. L. Donley, J. Zaumseil, J. W. Andreasen, M. M. Nielsen, H. Sirringhaus, R. H. Friend and J.-S. Kim, *J. Am. Chem. Soc.*, 2005, **127**, 12890-12899.
33. R. S. Ashraf, A. J. Kronemeijer, D. I. James, H. Sirringhaus and I. McCulloch, *Chem. Commun.*, 2012, **48**, 3939-394.

34. A. J. Kronemeijer, E. Gili, M. Shahid, J. Rivnay, A. Salleo, M. Heeney and H. Sirringhaus, *Adv. Mater.* 2012, **24**, 1558–1565.
35. Y. Kim, H. R. Yeom, J. Y. Kim and C. Yang, *Energy Environ. Sci.* 2013, **6**, 1909-1916.

Captions of Figures

Scheme 1. Synthetic route of the BDPT-based SMs.

Fig. 1. Crystal structure of BDPT (a) and the intermolecular arrangements in the crystal (b), H-atoms are omitted for clarity.

Fig. 2. TGA (a) and DSC (b) curves of the BDPT-based SMs.

Fig. 3. UV-vis absorption spectra of the BDPT-based SMs in chloroform solution (a) and in thin film (b).

Fig. 4. CV curves of the BDPT-based SMs.

Fig. 5. Top view and side view of optimized geometries for the BDPT-based SMs. Color code: gray (C), white (H), red (O), blue (N), orange (S) and yellow (F).

Fig. 6. $J-V$ characteristics of the SMs/PC₇₁BM-based solar cells at the blend ratio of 1:1 .

Fig. 7. X-ray diffraction patterns of the SMs/PC₇₁BM blend films with/without 1% DIO at optimized blend ratio.

Fig. 8. TEM images of the SM/PC₇₁BM blend films: (a) BDPT-2BT/ PC₇₁BM (1:1), (b) BDPT-2FBT/PC₇₁BM (1:1), (c) BDPT-2DPP/PC₇₁BM (1:1), (d) BDPT-2DPP/PC₇₁BM (1.5:1) and (e) BDPT-2BT/PC₇₁BM (1:1) with 1% DIO, (f) BDPT-2FBT/PC₇₁BM (1:1) with 1% DIO, (g) BDPT-2DPP/PC₇₁BM (1:1) with 1% DIO, (h) BDPT-2DPP/PC₇₁BM (1.5:1) with 1% DIO, respectively. The scale bars represent 200 nm.

Fig. 9. EQE curves of the SMs/PC₇₁BM blend films at the optimized blend ratio and DIO additive.

Fig. 10 $J-V$ characteristics of the hole-only SMs/PC₇₁BM-based device. The solid lines represent the best linear fit of the data points.

Table 1. Optical and electro-chemical properties of the BDPT-based SMs.

Table 2. Photovoltaic properties of the SMs/PC₇₁BM-based solar cells.

Scheme 1.

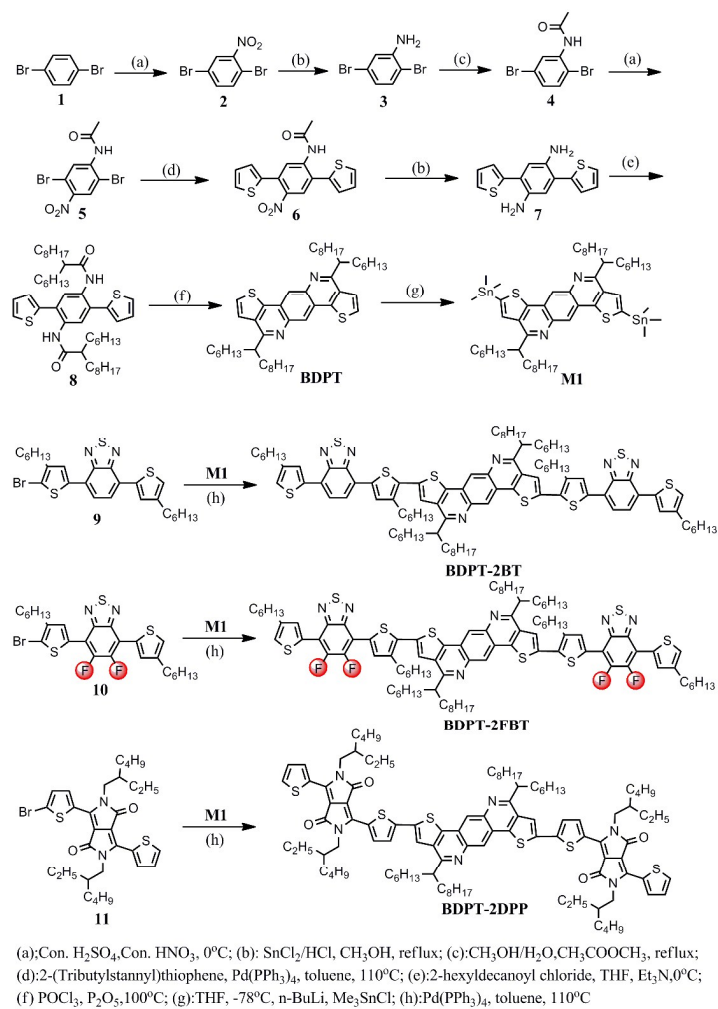


Fig. 1

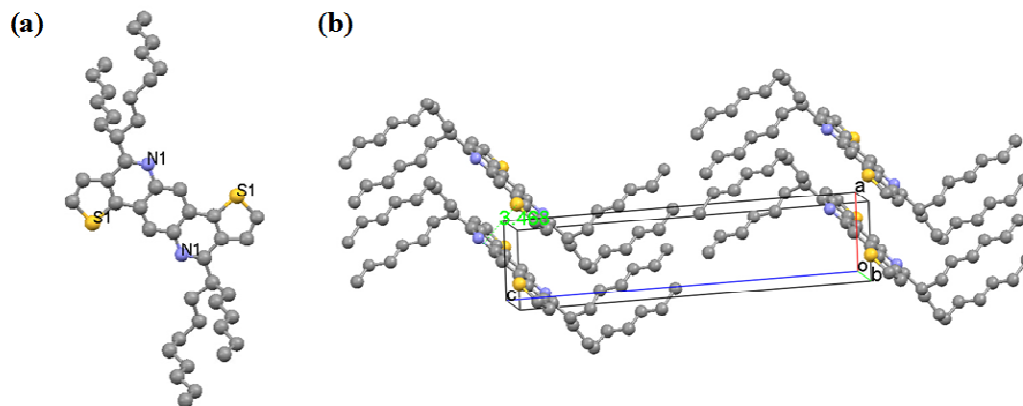


Fig. 2.

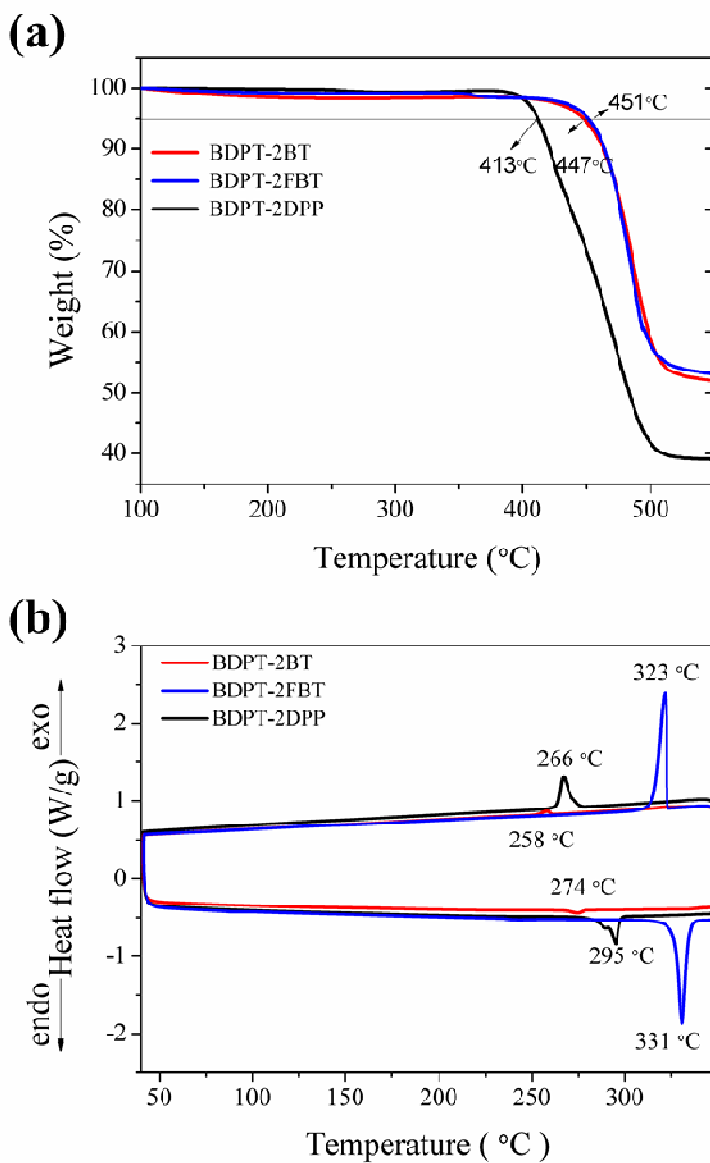


Fig. 3.

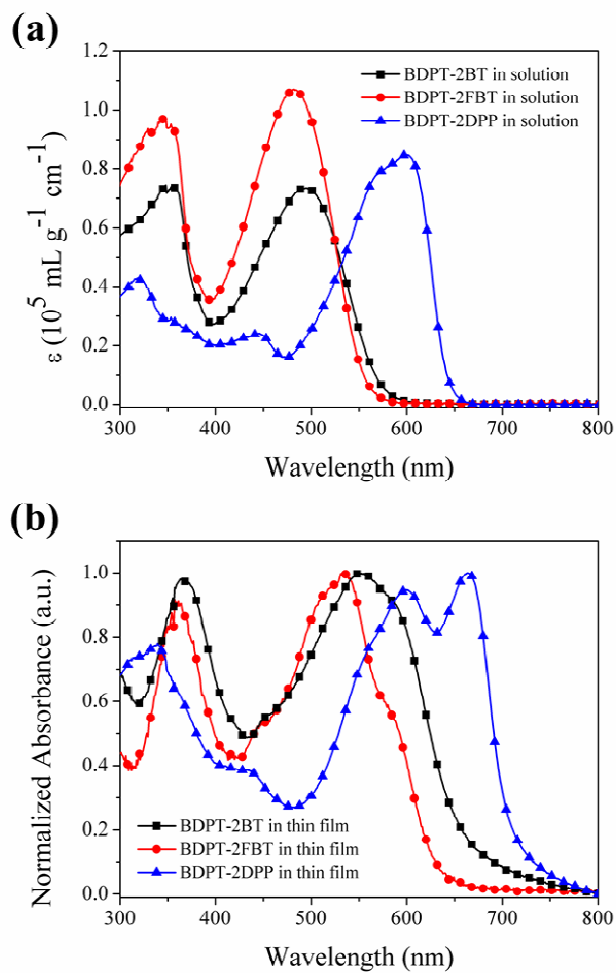


Fig. 4.

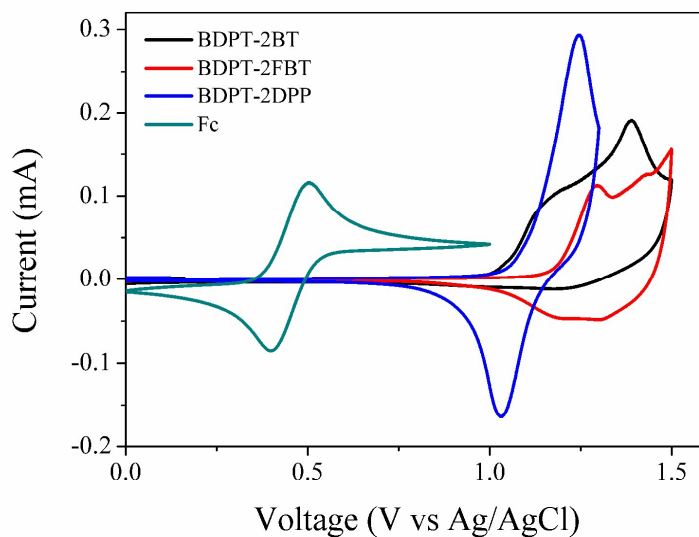


Fig. 5.

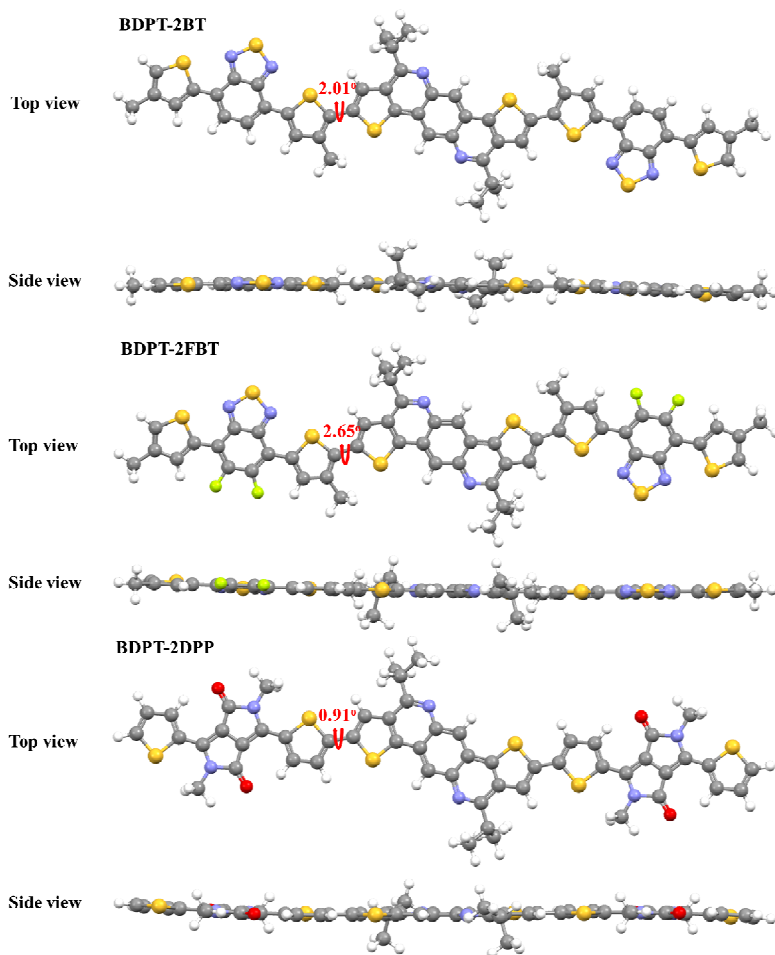


Fig. 6.

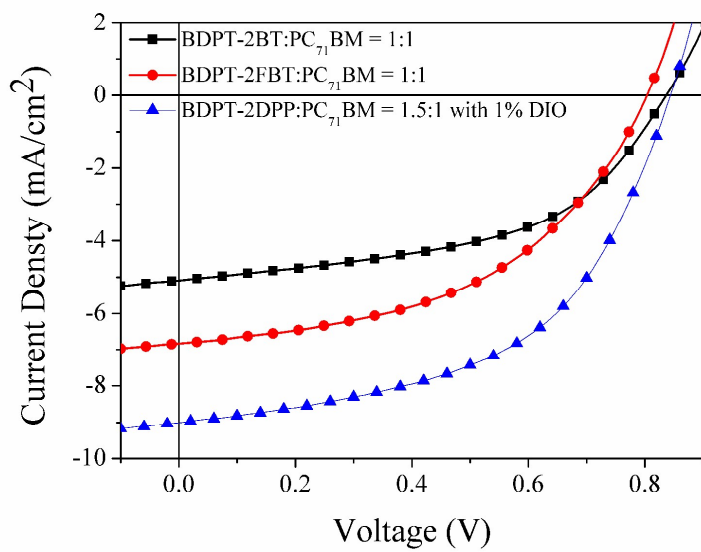


Fig. 7.

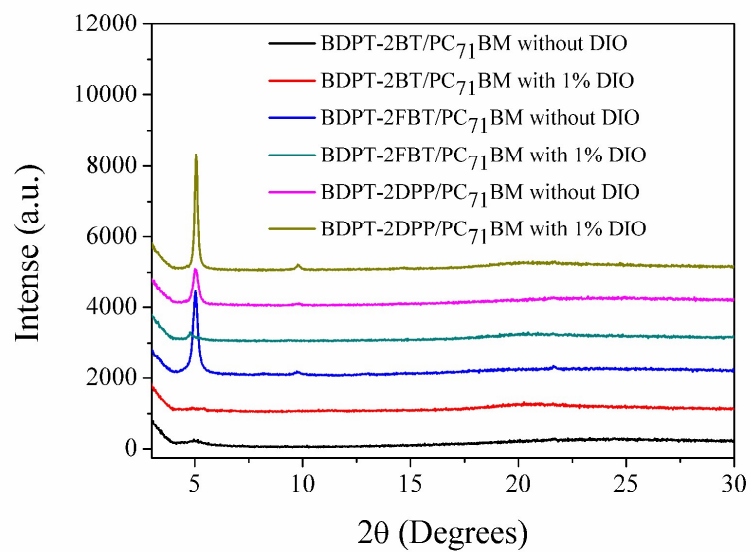


Fig. 8.

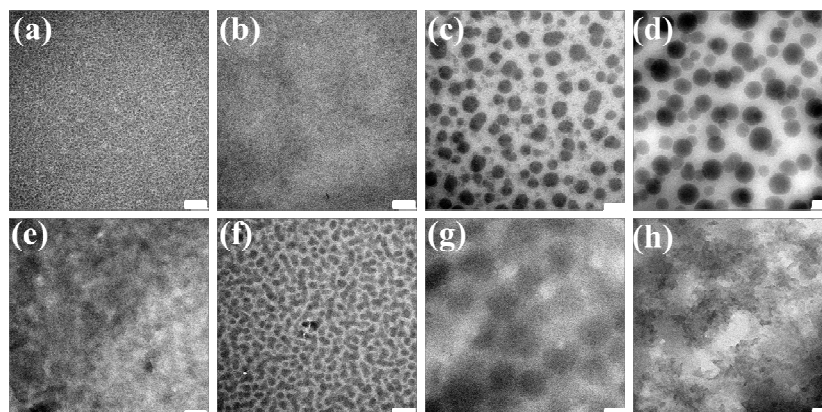


Fig. 9.

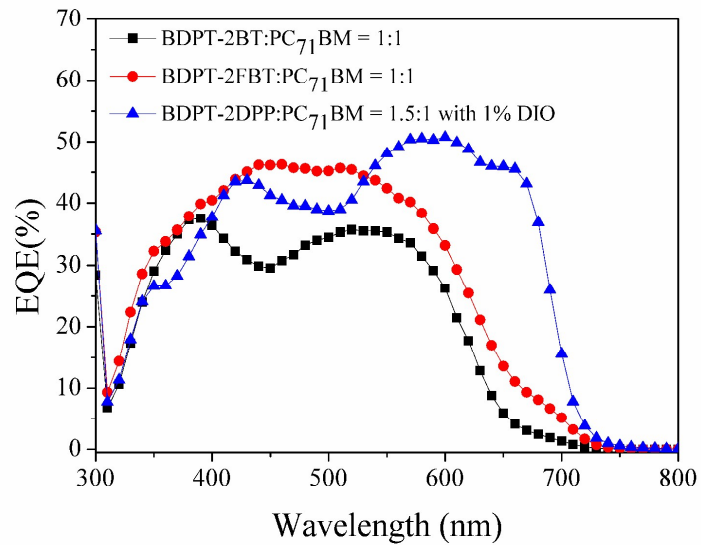


Fig. 10.

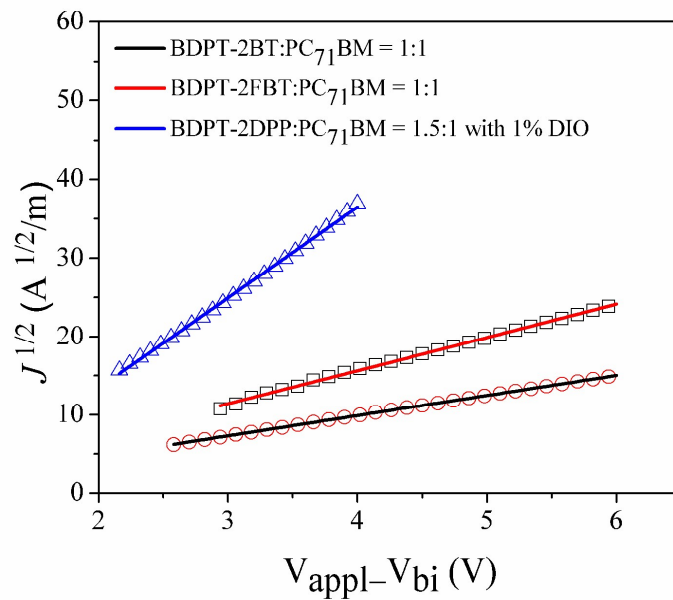


Table 1.

SMs	λ_{\max} (nm)		λ_{onset} (nm)	E_g^{opt}	E_{HOMO}	E_{LUMO}	
	Solution ($\epsilon \times 10^4$)		film	film	(eV) ^a	(eV) ^b	(eV) ^c
BDPT-2BT	350 (9.5), 492 (10.2)		363, 556, 587	652	1.90	-5.38	-3.48
BDPT-2FBT	345 (7.4), 482 (7.2)		360, 537, 580	630	1.97	-5.55	-3.58
BDPT-2DPP	332 (4.3), 600 (8.4)		337, 600, 663	710	1.75	-5.44	-3.69

^aCalculated from the absorption band edge of the films, $E_g = 1240/\lambda_{\text{onset}}$

^bCalculated from empirical equation: $E_{\text{HOMO}} = -(E_{\text{ox}} + 4.37)$ eV

^cCalculated from $E_{\text{LUMO}} = E_{\text{HOMO}} + E_g^{\text{opt}}$

Table 2.

SMs	D/A ratio	DIO ratio	V_{oc} (V)	J_{sc} (mA/cm ²)	FF (%)	PCE (%)	μ_{h} [cm ² v ⁻¹ s ⁻¹]
BDPT-2BT	1:1	No	0.84	5.08	51.25	2.18	2.94×10^{-6}
BDPT-2FBT	1:1	No	0.80	6.83	48.07	2.63	1.66×10^{-5}
BDPT-2DPP	1.5 : 1	1%	0.84	9.0	52.37	3.97	1.05×10^{-4}